


Research Article

On the Seismic Performance of the Single-Layer Reticulated Shell with a Center-Hung Scoreboard under Multiple Seismic Excitations

Renjie Liu ¹, Ce Ji,¹ Xiongyan Li,² Chao Wang,¹ and Guangyong Wang¹

¹School of Civil Engineering, Yantai University, Yantai 264005, China

²Spatial Structures Research Center, Beijing University of Technology, Beijing 100124, China

Correspondence should be addressed to Renjie Liu; renjie.liu@ytu.edu.cn

Received 8 November 2022; Revised 13 January 2023; Accepted 13 January 2023; Published 3 February 2023

Academic Editor: Denise-Penelope Kontoni

Copyright © 2023 Renjie Liu et al. This is an open access article distributed under the Creative Commons Attribution License, which permits unrestricted use, distribution, and reproduction in any medium, provided the original work is properly cited.

Single-layer reticulated shells are widely used as roof structures of gymnasiums. However, the seismic performance of the single-layer reticulated shell with a center-hung scoreboard (CHS), which is a kind of large-scale display device suspended on the roof center of many gymnasiums, has not been fully studied. In this paper, the influence of the CHS on the seismic response of single-layer reticulated shells is investigated. Single-layer reticulated shells and the CHS-integrated models including flexibly suspended models and simplified models are established, respectively, using the Abaqus software. The responses of integrated models are calculated by an explicit dynamic method under 3D seismic action. The axial forces of the flexibly suspended case and the simplified case where the scoreboard is simplified as fixed masses on the roof structure are compared. Compared with those in the simplified model, the axial forces of some shell members and some nodal acceleration in the flexibly suspended model under multiple seismic excitations would increase by as high as 125% and 315%, respectively. It turns out that seismic responses of the single-layer reticulated shell would be underestimated if a simplified model was used for seismic response analysis. The region near the boundary and the region neighbouring the support platform members are the most affected regions due to the combination of the horizontal swing effect and the vertical impact effect of the CHS under multiple seismic excitations.

1. Introduction

Single-layer reticulated shells have characteristics of reasonable stiffness and diverse shapes and are widely used as roof structures of gymnasiums. Since single-layer reticulated shells have characteristics of the dense frequency and complex seismic response [1], research on the seismic response of single-layer reticulated shells is a hot spot in the field of spatial structures.

The research on the seismic response of single-layer reticulated shells has reached many achievements. Incremental dynamic analysis on single-layer spherical reticulated shells was conducted, and it was found that factors such as roof quality, rise-span ratio, and span have nonnegligible effects on the seismic response [2]. The seismic response of

nine reticulated shells under 40 far-field and near-field ground motions was analysed, and it was found that near-field ground motions caused more serious damage [3]. The seismic performance of the reticulated shells based on the energy method was studied, and it was found that if the earthquake duration is too short, there would be unsafe hidden dangers such as overestimating the dynamic bearing capacity and underestimating the plastic development degree [4]. The influence of column supports on the seismic performance of the single-layer reticulated shells with FPBs was studied by Kong et al. [5]. Friction pendulum bearings can make the natural vibration period far away from the predominant period of the seismic wave, thus avoiding the occurrence of resonance between the shell structure and the seismic wave. Yu et al. found that the effect of supporting

flexibility significantly influences the failure characteristics of single-layer reticulated domes subjected to severe earthquakes [6].

The dynamic stability of the K6 single-layer spherical reticulated shell under asymmetric loads was analysed by Zhou et al. [7]. The research shows that the influence of the form and size of loads and the spectral characteristics of seismic waves on the dynamic stability of reticulated shells cannot be ignored. Zhi et al. [8] found that the roof system can effectively improve the overall stiffness of single-layer spherical reticulated shells and enhance the seismic capacity of the structure. Zhang et al. [9, 10] studied the effects of different initial geometric defect modes on the seismic performance of single-layer reticulated shells and the influence of different initial geometric defects on the seismic bearing capacity of single-layer spherical reticulated shells and found that the most unfavorable defects of reticulated shells generally appear in high-order buckling modes. Zhi et al. [11] obtained indicators to measure the ability to resist earthquakes. Nie et al. [12] found that, after considering the coupling effect between the lower support and the single-layer cylindrical reticulated shell, the dynamic strength failure of the reticulated shell occurs with the strong lower support, and the lower support dynamic strength failure occurs with the weak support structure. Yang et al. [13] pointed out that the long-span reticulated shell structure with a separated lower support design has good seismic performance. Yu et al. [14] proposed a method to judge the strong earthquake failure of single-layer cylindrical aluminium alloy reticulated shells and found that the aluminium alloy-reticulated shell structure has good seismic performance.

On the whole, the current seismic response analysis methods of the reticulated shell include the mode decomposition response spectrum method, time-history method, incremental dynamic analysis method, and push-over method [15]. At present, factors such as the rise-to-span ratio, initial defects, support conditions, and multidimensional seismic action of the earthquake should not be ignored in the seismic response analysis of single-layer reticulated shells. However, all these findings are based on the seismic performance of reticulated shells without a center-hung scoreboard (CHS) which is a large-scale display device flexibly suspended in the center of the gymnasium [16, 17], as shown in Figure 1.

In recent years, with the development of professional sports events and other activities, the number of CHS applications has increased significantly. For better display performance, the CHS is developing towards larger display areas and smaller pixel pitches, and its weight increases accordingly. The heaviest CHS is about 55 t [16, 17]. However, there are few research achievements considering the influence of the flexibly suspended CHS on the seismic response of single-layer reticulated shells in current studies. Liu et al. [18] analysed the influence of the CHS on natural dynamic characteristics of single-layer reticulated shells and found that the influence on dynamic characteristics cannot be ignored, especially for low-order frequencies and mode shapes. The influence of



FIGURE 1: New center-hung scoreboard for the Thomas and Mack Center.

the CHS on the seismic response of single-layer spherical reticulated shells under a one-dimensional horizontal earthquake was investigated; the swing effect of the CHS could cause an increase by more than 100% on both the acceleration and internal forces [19]. Ding et al. [20] analysed the seismic response of large-span spatial structures under three-dimensional orthogonal ground motion excitation. The seismic response of the roof structure of the Tianjin Olympic Center Stadium under the uniform excitation of one-dimensional random ground motion or three-dimensional random ground motion is analysed by numerical simulations. The results show that considering the spatial effect of ground motion, the internal force of the structural control member will increase by about 30%, considering the partial coherence effect, the internal force of the structural member will change by about 10%, and considering the multidimensional seismic input, the internal force of the structural control member will increase by about 15%. Therefore, for seismic response analysis of long-span spatial structures, multidimensional input of ground motion must be considered. The influence of the CHS on the seismic response of single-layer spherical reticulated shells under one-dimensional vertical seismic action was studied; the vertical impact effect of the CHS could cause a significant increase in both the acceleration and internal forces [21]. In all, the seismic response would be significantly underestimated if a simplified model, in which the CHS was simplified as fixed masses on structure nodes, was used. However, current research on the influence of the CHS on the seismic response of the reticulated shell is about one-dimensional seismic excitation. It makes sense to reveal the mechanism how the CHS influences the seismic response in the study of one-dimensional seismic action. In terms of structural design for engineering, neglecting spatial variation of ground motions would underestimate the seismic response of spatial space truss structures [22].

In this paper, the seismic performance of the single-layer reticulated shell with a CHS under multiple seismic action is investigated. Flexibly suspended models and simplified models are built using the Abaqus software, respectively. The seismic response of the two kinds is compared and discussed. The influence of the weight and the sling length of the CHS on the seismic response of the single-layer spherical reticulated shell is analysed.

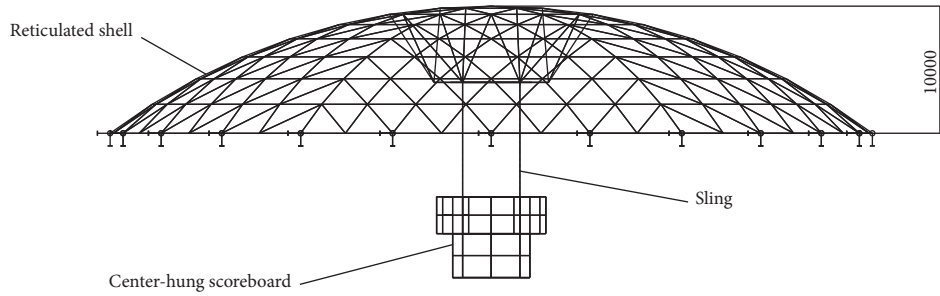


FIGURE 2: Front view of the integrated model.

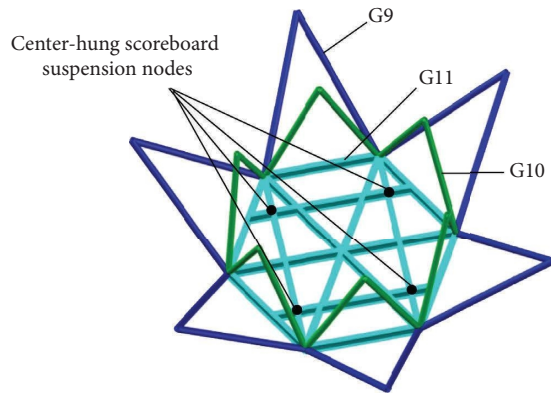


FIGURE 3: The support platform for the CHS.

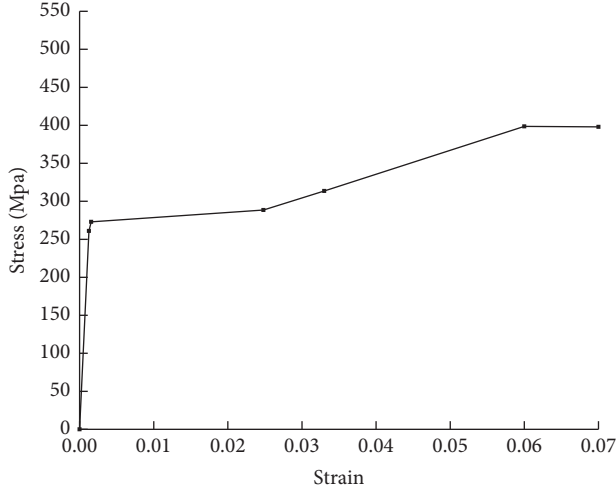


FIGURE 4: Stress-strain curve of the steel Q355B.

2. Models and Methods

2.1. FE Models. A single-layer spherical $K6$ reticulated shell with a diameter of 60 m and a rise-span ratio of 1/6 is used as a roof structure of a gymnasium, as shown in Figure 2. A support platform is located in the center of the shell for lifting the CHS, as shown in Figure 3. The support platform and the shell are connected by steel rods. The CHS and the support platform are connected by slings, and the vertical location of the CHS can be controlled by using a hoist system. Vertical rods between the reticulated shell and the

TABLE 1: Section specifications of structural members.

Section number	Section specifications	Materials
G1	$\phi 273 \times 12$	Q355B
G2	$\phi 273 \times 14$	
G3	$\phi 245 \times 14$	
G4	$\phi 245 \times 12$	
G5	$\phi 230 \times 12$	
G6	$\phi 219 \times 12$	
G7	$\phi 219 \times 10$	
G8	$\phi 325 \times 16$	
G9	$\phi 273 \times 10$	
G10	$\phi 245 \times 10$	
G11	HN550 \times 200	
S1	$\phi 12$	

The section specification of the circular pipe: $\phi 245 \times 10$ means that the outer diameter is 245 mm and the thickness is 10 mm. The section specification of the spiral strand: $\phi 12$ means that the nominal diameter is 12 mm.

support platform are made of Q355B circular pipes, platform-crossing members are made of Q355B-rolled H beams, and slings are made of high vanadium-coated cables. Chen et al. [23] used an Instron tensile testing machine to carry out the quasi-static tensile test on Q345 steel. The LS-DYNA module in ANSYS was used to simulate the tensile test under different loading rates. The true stress-strain curve of the steel was obtained by combining the test and simulation. The strain-stress curve of the Q355B steel is shown in Figure 4. The Abaqus software is used for FE analysis. The explicit beam element was used for shell members and platform members, and the explicit truss element was used for slings. The section specifications of the structural members are shown in Table 1 and Figures 3 and 5. Similar to the mass pendulum, the sling length and the weight of the CHS are the main parameters that affect dynamic characteristics; different sling lengths and different weights are designed to study influence laws. In practice, a safety distance of about 1.0 m is reserved between the CHS and the support platform, and a sling length is selected every 0.5 m between 1.0 m and 9.0 m. The length of the sling is taken as 0.0 m when the CHS is simplified as fixed masses on the suspension nodes on the support platform. Since most of the CHSs used in recent years exceed 20 t and the heaviest ones have exceeded 55 t [16, 17], the weight is selected every 5 t between 20 t and 60 t. The standard value of the dead load D includes the standard value of uniformly distributed dead loads on the roof, which

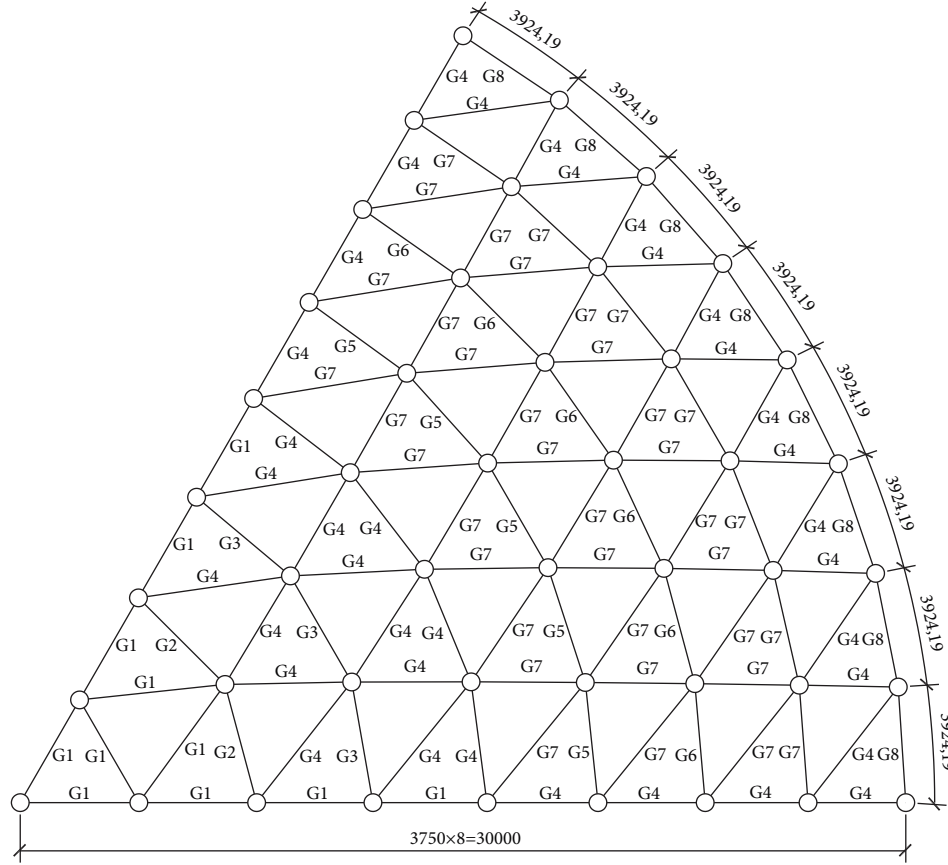


FIGURE 5: The layout of the shell members.

is 1.0 kN/m^2 , and the self-weight of members and nodes. The standard value of a uniformly distributed live load on the roof L is taken as 0.5 kN/m^2 , and the representative value of a gravity load is $1.0D + 0.5L$. The boundary conditions are assumed to be three-way fixed hinge supports (Figure 2). The representative value of a gravity load of the roof without the CHS is about 500 t. The weight of the CHS between 20 t and 60 t is about 1/15 to 1/9 of the representative value of the gravity load of the roof.

2.2. Seismic Response Analysis Methods. Commonly used seismic response analysis methods for large-span spatial structures include the mode shape decomposition response spectrum method, time-history analysis method, and simplified analysis method provided by the regulations [24]. The time-history analysis method is a direct dynamic analysis method, which can analyse both the linear elastic dynamic response and the elastic-plastic dynamic response [25].

The differential equation of elastic motion of the coupled system is shown in Equation (1), where $[M]$, $[C]$, and $[K]$ are the mass matrix, damping matrix, and stiffness matrix, respectively, $\{\ddot{u}\}$, $\{\dot{u}\}$, and $\{u\}$ are the acceleration vector, velocity vector, and displacement vector, respectively, and $\{\ddot{u}_g(t)\}$ is the ground motion acceleration array.

$$[M]\{\ddot{u}\} + [C]\{\dot{u}\} + [K]\{u\} = -[M]\{\ddot{u}_g(t)\}. \quad (1)$$

When the members of the coupled system enter the elastic-plastic stage, the damping matrix $[C]$, and the overall stiffness matrix $[K]$ will change with time t . The premise of Rayleigh damping is that the damping is assumed to have a linear proportional relationship with mass and stiffness, which is similar to some extent. It is well known that the damping matrix $[C]$ itself is a “macro and comprehensive” uncertainty and that the inverse damping matrix itself is an approximate process. From this point of view, Rayleigh damping is complete in theory and is in good agreement with the experimental and measured results. Therefore, Rayleigh damping is selected for the damping matrix $[C]$. The differential equation of elastic-plastic motion of the coupled system becomes the following equation:

$$[M]\{\Delta\ddot{u}\} + [C]\{\Delta\dot{u}\} + [K]\{\Delta u\} = -[M]\{\Delta\ddot{u}_g\}, \quad (2)$$

$$\{\Delta\ddot{u}\} = \{\ddot{u}(t + \Delta t)\} - \{\ddot{u}(t)\}, \quad (3)$$

$$\{\Delta\dot{u}\} = \{\dot{u}(t + \Delta t)\} - \{\dot{u}(t)\}, \quad (4)$$

$$\{\Delta u\} = \{u(t + \Delta t)\} - \{u(t)\}. \quad (5)$$

Commonly used integration algorithms include implicit algorithms and explicit algorithms. The static equilibrium equation needs to be solved iteratively at each incremental step in the implicit algorithm. In the flexibly

suspended model, the CHS hangs using only tension slings, the model is a mechanism, and the overall stiffness matrix is singular. Therefore, the implicit algorithm is not suitable for solving such problems. The explicit algorithm does not need to directly solve tangent stiffness or balance iteration and is highly applicable to the analysis of the seismic response in the flexibly suspended model. The explicit solution uses the central difference method to complete the simulation with multiple time increments. Explicitly, it only focuses on the state of the previous moment. The solution of each step is based on the result of the previous step, and the subsequent result is recursive by the preset time increment. The explicit algorithm has conditional stability but has no computational convergence problem. Therefore, the dynamic explicit analysis in the Abaqus software is used for calculating the seismic response. The shaking table test of a 1 : 20 scale model of a suspend-dome structure with a large CHS is carried out to verify the numerical modeling method and the validity of the numerical model. However, this study only focuses on the suspend-dome structure, and the research on single-layer spherical reticulated shells has not been involved. [26, 27].

2.3. Selection of Seismic Waves. In general, the seismic waves available for structural time-history analysis include actual seismic records of the proposed site, typical past seismic records, and artificial seismic waves. According to provisions of the regulation [25], when the time-history analysis method is used, the actual strong earthquake records and the artificially simulated acceleration time-history curve should be selected according to the type of the construction site and the design earthquake group, and the number of actual strong earthquake records should not be less than 2/3 of the total number; the average seismic influence coefficient curve of multiple sets of time-history curves should be consistent with the seismic influence coefficient curve used by the mode shape decomposition response spectrum method in a statistical sense. When three sets of acceleration time-history curves are input, the calculation result should take the envelope value of the time-history method.

Three elements of ground motion should be fully considered when selecting seismic waves, including ground motion intensity, ground motion spectral characteristics, and ground motion duration. The ground motion intensity is generally the acceleration peak value, and the amplitude is modulated according to the acceleration peak value corresponding to the corresponding fortification intensity; the acceleration peak value is adjusted as

$$a_0(t_i) = \frac{a_{0,\max}}{a_{\max}} a(t_i). \quad (6)$$

In the formula, $a_0(t_i)$ and $a_{0,\max}$ are the seismic acceleration curve and the peak value after adjustment, respectively, and $a(t_i)$ and a_{\max} are the seismic acceleration curve and the peak value of the original record, respectively.

Considering the spectral characteristics of ground motion, the predominant period of the selected seismic wave is as consistent as possible with the design characteristic

period, and the epicentral distance of the selected seismic wave is as consistent as possible with that of the proposed site. The design conditions of site Class II, the design earthquake group is the second group, the seismic fortification intensity is 8 degrees, and the design basic acceleration is 0.3 g, are taken as an example.

Natural seismic waves (El Centro, Taft, and artificial RH4TG040) are selected. The acceleration time-history curves are shown in Figures 6–9. Figure 9 shows that the seismic wave response spectrum curves after amplitude modulation are in agreement with the design response spectrum curve and the average seismic wave response spectrum curve.

2.4. Seismic Wave Input Method. If the seismic fortification intensity is 8 degrees, for the spatial grid structure such as the single-layer reticulated shell structure, the vertical and horizontal seismic effects should be checked [24, 25]. In addition, since the span of the models is 60 meters, the traveling wave effect is not very significant. The consistent input method is adopted for seismic wave input. The seismic acceleration peak value in three directions is adjusted according to 1 (horizontal 1), 0.85 (horizontal 2), and 0.65 (vertical). The influence of other input methods on the seismic response of the single-layer reticulated shells will be studied separately in the future.

3. Results and Discussion

The influence of the axial forces on reticulated shell members is mainly concerned since underestimation or overestimation of the internal forces is related to the safety of structural member design. The axial forces of the flexibly suspended cases and the simplified cases where the scoreboard is simplified as fixed masses on the support platform are compared. The degree that the axial forces are affected and the position of the reticulated shells where the axial forces are most affected are analysed. Deep mechanisms as to how the CHS affects seismic responses are discussed based on both axial forces and nodal acceleration. The influence laws of the sling length and the scoreboard weight on the responses are also discussed.

3.1. Degree of the Influence on Axial Forces. The envelope peak values of the time history of axial forces under three sets of seismic waves are taken as the peak axial force of a structural member. The symbol $F_{j,\max}^{w,l}$ is set as the peak axial force of the j th member when the weight of the CHS is w and the sling length is l , where j is a positive integer. Then, the change rate $\gamma_{j,\max}^{w,l}$ of the j th member can be obtained by Equation (7), where the symbol $F_{j,\max}^{w,0}$ represents the peak axial force when the weight of the CHS is w , and the CHS is simplified as fixed masses on the support platform. The maximum change rate $\gamma_{\max}^{w,l}$ and the minimum value $\gamma_{\min}^{w,l}$ of the axial forces of the single-layer reticulated shell members are calculated, respectively, by Equations (8) and (9), for analysing the degree of the influence of w and l on the axial

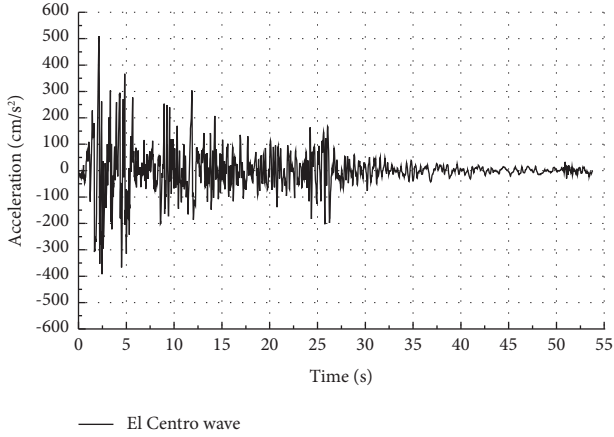


FIGURE 6: Time-history curve of El Centro waves.

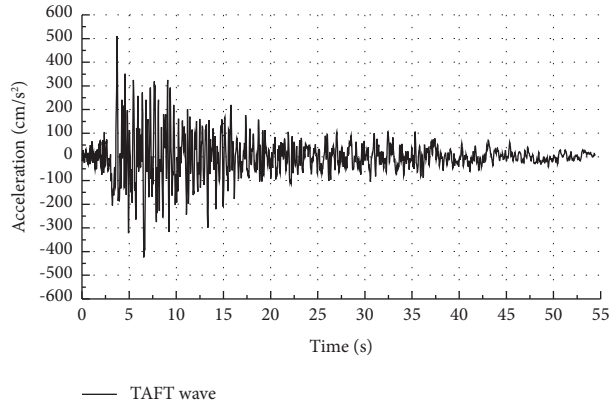


FIGURE 7: Time-history curve of Taft waves.

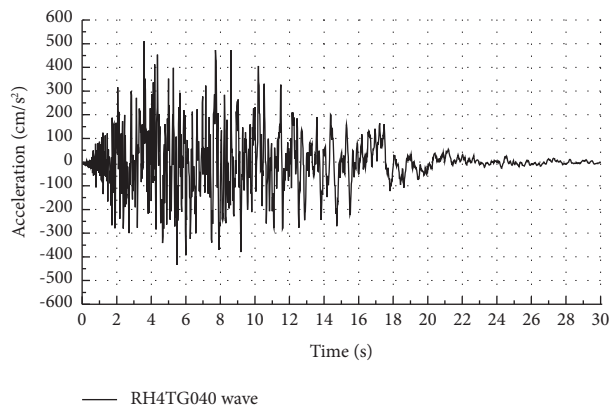


FIGURE 8: Time-history curve of RH4TG040.

forces of all members, where p is the total number of members in the shell.

$$\gamma_{j, \max}^{w,l} = \frac{F_{j, \max}^{w,l} - F_{j, \max}^{w,0}}{F_{j, \max}^{w,0}}, \quad (7)$$

$$\gamma_{\max}^{w,l} = \max_{j=1 \sim p} \{\gamma_{j, \max}^{w,l}\}, \quad (8)$$

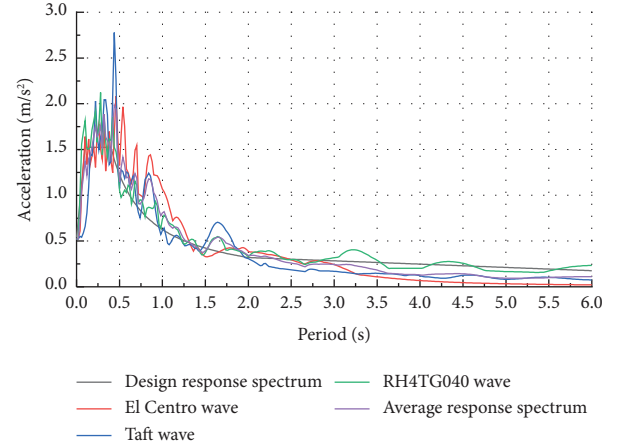


FIGURE 9: Response spectrum curves.

$$\gamma_{\min}^{w,l} = \min_{j=1 \sim p} \{\gamma_{j, \max}^{w,l}\}. \quad (9)$$

Figure 10 shows that $\gamma_{\max}^{w,l}$ of different reticulated shell members are between 57.7% and 125%. It indicates that the axial forces of some shell members would increase by as high as 125%. Figure 11 shows that the minimum change rate $\gamma_{\min}^{w,l}$ of the reticulated shell members is between -46% and -24.3%. It indicates that the axial forces of some shell members would decrease by as high as 46%. Hence, the seismic response would be greatly different between the flexibly suspended model and the simplified model. The axial forces of some reticulated shell members would be underestimated if a simplified model was used for seismic response analysis.

It is shown in Figure 10 that the maximum change rate $\gamma_{\max}^{w,l}$ occurs when the weight of the CHS is 20 t and the sling length is 4.0 m. When w is between 30 t and 40 t, $\gamma_{\max}^{w,l}$ is basically maintained at the lowest level. When w is between 30 t and 45 t, $\gamma_{\max}^{w,l}$ of the reticulated shell members are less affected by the weight and the length, and $\gamma_{\max}^{w,l}$ is maintained below 85%. When w is between 35 t and 60 t, $\gamma_{\max}^{w,l}$ of the reticulated shell member is less affected by the weight and the length, and $\gamma_{\max}^{w,l}$ is maintained between 85% and 100%. The $\gamma_{\max}^{w,l}$ value gradually decreases with an increase in w and l . When the length is between 2.0 m and 5.0 m, $\gamma_{\max}^{w,l}$ changes significantly. It is shown in Figure 11 that maximum $\gamma_{\min}^{w,l}$ appears when w is 50 t and l is 2.5 m, and minimum $\gamma_{\min}^{w,l}$ appears when w is 40 t and l is 4.0 m. When w is greater than 40 t, with an increase in l , $\gamma_{\min}^{w,l}$ of the reticulated shell members increases first and then decreases. When l is less than 4.0 m, with an increase in w , $\gamma_{\min}^{w,l}$ increases gradually. When l is greater than 4.0 m, $\gamma_{\min}^{w,l}$ increases first and then decreases with an increase in l .

Compared with the results under one-dimensional horizontal seismic excitation or vertical seismic action, the influence laws of the weight and the length under multiple seismic action are complicated. The deep mechanism of the complicated laws is due to the combination of horizontal

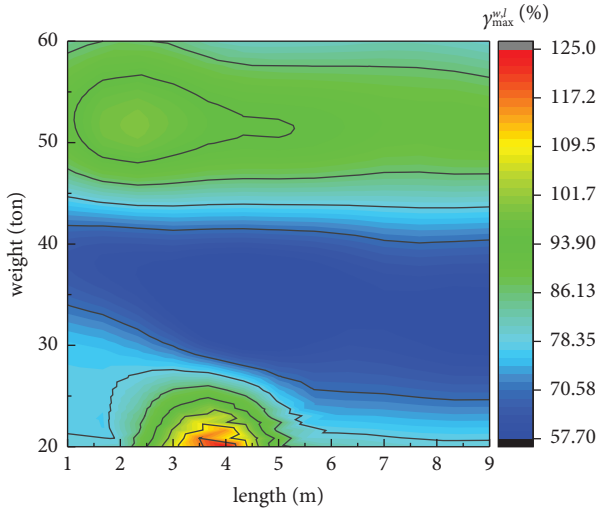


FIGURE 10: The $\gamma_{j,max}^{w,l}$ values of the shell members.

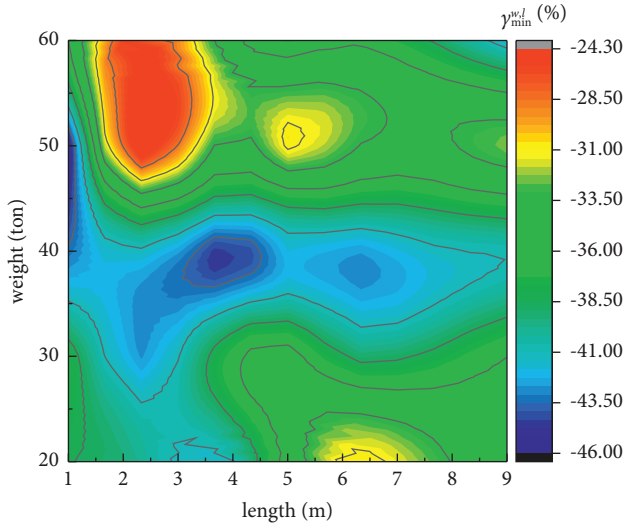


FIGURE 11: The $\gamma_{j,min}^{w,l}$ values of the shell members.

swing effects and vertical impact effects of the CHS under multiple seismic action and the complicated dynamic characteristics controlled by the CHS weight and the sling length. However, Figures 10 and 11 show only the overall degree of the influence of the CHS on the axial forces of the shell members with the variation of the weight and the length. The position of the reticulated shells where the axial forces are most affected needs to be displayed.

3.2. The Position of the Most Affected Shell Members. In order to display the position of the most affected shell members, contours of the change rate $\gamma_{j,max}^{w,l}$ of shell members are shown in Table 2. The change rate $\gamma_{j,max}^{w,l}$ for most reticulated shell members is maintained at a low level, below 40%, but the distribution of $\gamma_{j,max}^{w,l}$ is complicated with different weight and different sling length. The reticulated shell members with a $\gamma_{j,max}^{w,l}$ value over 50% locate at two parts

including the region near the boundary and the region neighbouring support platform members. The reason why the shell members near the boundary are greatly affected is the swing effect of the CHS caused by the horizontal component of multiple seismic excitations. The boundary bears more horizontal reaction forces than the simplified model. The combination of the swing effect caused by the horizontal component and the vertical impact effect caused by the vertical component causes the region neighbouring support platform members to be the most affected part.

It is displayed that the parameters w and l significantly affect the distribution of the change rate $\gamma_{j,max}^{w,l}$ of the reticulated shell members, but the influence laws are complicated. There are many types of single-layer reticulated shells and the shells of one type are usually unique with different parameters in practice, so it is hard to find general rules for all single-layer reticulated shells.

3.3. Influence on Nodal Acceleration. The influence of the CHS on nodal acceleration in three components is also discussed for illustrating the deep mechanism how the CHS affects the seismic responses. With the same theory for numbering the change rate of axial forces, the acceleration of the i th node for the reticulated shells is set as $a_{i,max}^{w,l}$ and the peak acceleration change rate of the i th node is $\rho_{i,max}^{w,l}$ which is obtained by Equation (10), where the symbol $a_{i,max}^{w,0}$ represents the peak acceleration when the weight of the CHS is w , and the CHS is simplified as fixed masses on the support platform. The $\rho_{i,max}^{w,l}$ and $\rho_{i,min}^{w,l}$ values of the acceleration in the reticulated shell are calculated, respectively, by Equations (11) and (12), where n represents the total number of nodes in the reticulated shell. The contours of the $\rho_{i,max}^{w,l}$, $\rho_{i,min}^{w,l}$, and $\rho_{i,max}^{w,l}$ values of the whole reticulated shell in the x -direction, y -direction, and z -direction are listed in Tables 3–5, respectively.

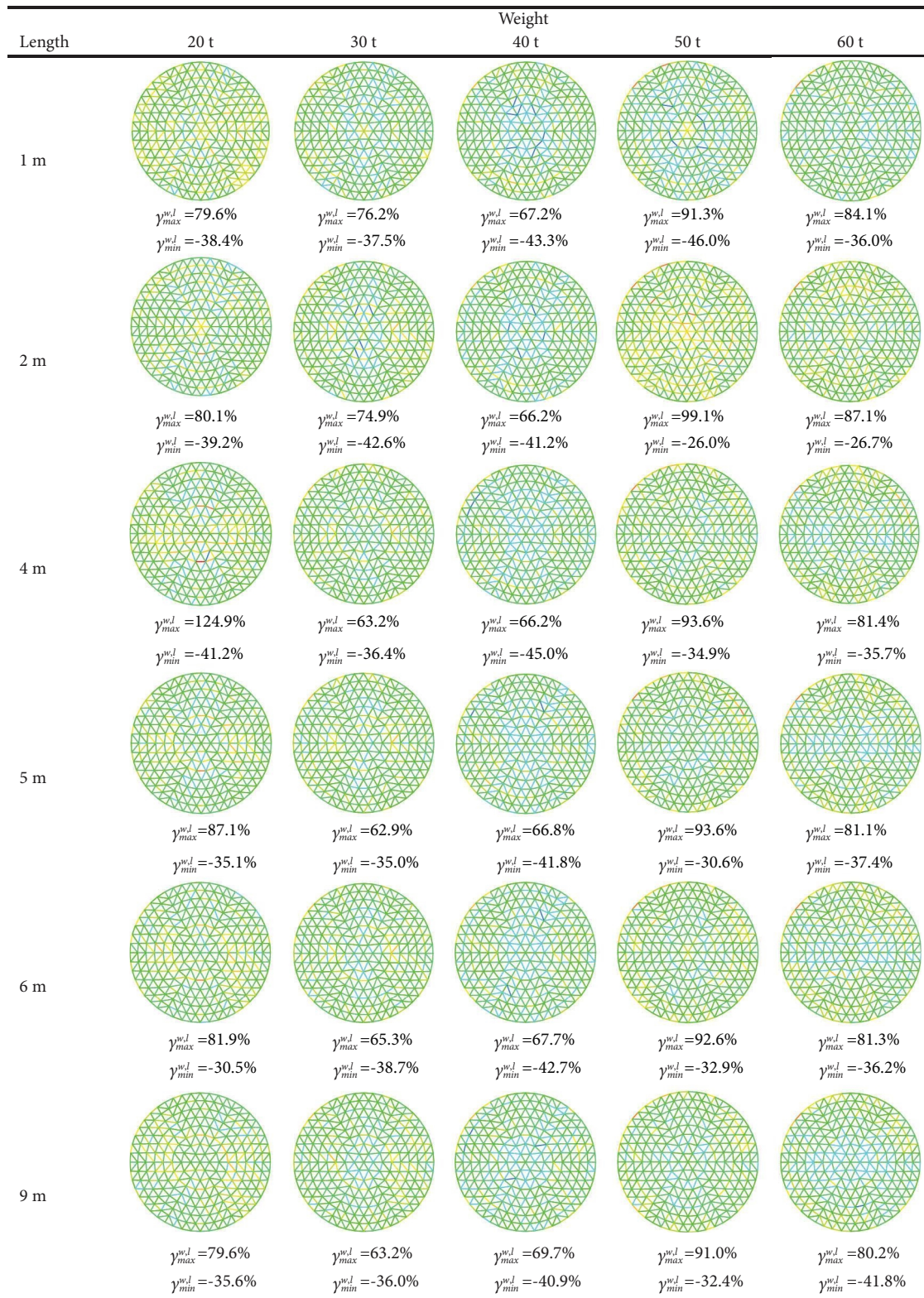
$$\rho_{i,max}^{w,l} = \frac{a_{i,max}^{w,l} - a_{i,max}^{w,0}}{a_{i,max}^{w,0}}, \quad (10)$$

$$\rho_{max}^{w,l} = \max_{i=1 \sim n} \{ \rho_{i,max}^{w,l} \}, \quad (11)$$

$$\rho_{min}^{w,l} = \min_{i=1 \sim n} \{ \rho_{i,max}^{w,l} \}. \quad (12)$$

It is shown in Table 3 that the $\rho_{max}^{w,l}$ values are between 98.4% and 146.2% and that the $\rho_{min}^{w,l}$ values are between -44.1% and -22.5% in the x -direction. Table 4 displays that the $\rho_{max}^{w,l}$ values are between 77.4% and 137.3% and that the $\rho_{min}^{w,l}$ values are between -47% and -6.6% in the y -direction. Table 5 depicts that the $\rho_{max}^{w,l}$ values are between 103.3% and 315% and that the $\rho_{min}^{w,l}$ values are between -40.7% and -6.2% in the z -direction. It indicates that nodal acceleration of the reticulated shell is greatly affected by the flexibly suspended CHS. Compared with that in the simplified model, the acceleration of some nodes increases by as high as 146.2%, 137.3%, and 315% in three components, respectively, in the flexibly suspended model. It also shows that

TABLE 2: Contours of the change rate $\gamma_{j, \max}^{w,l}$ of the reticulated shell members.

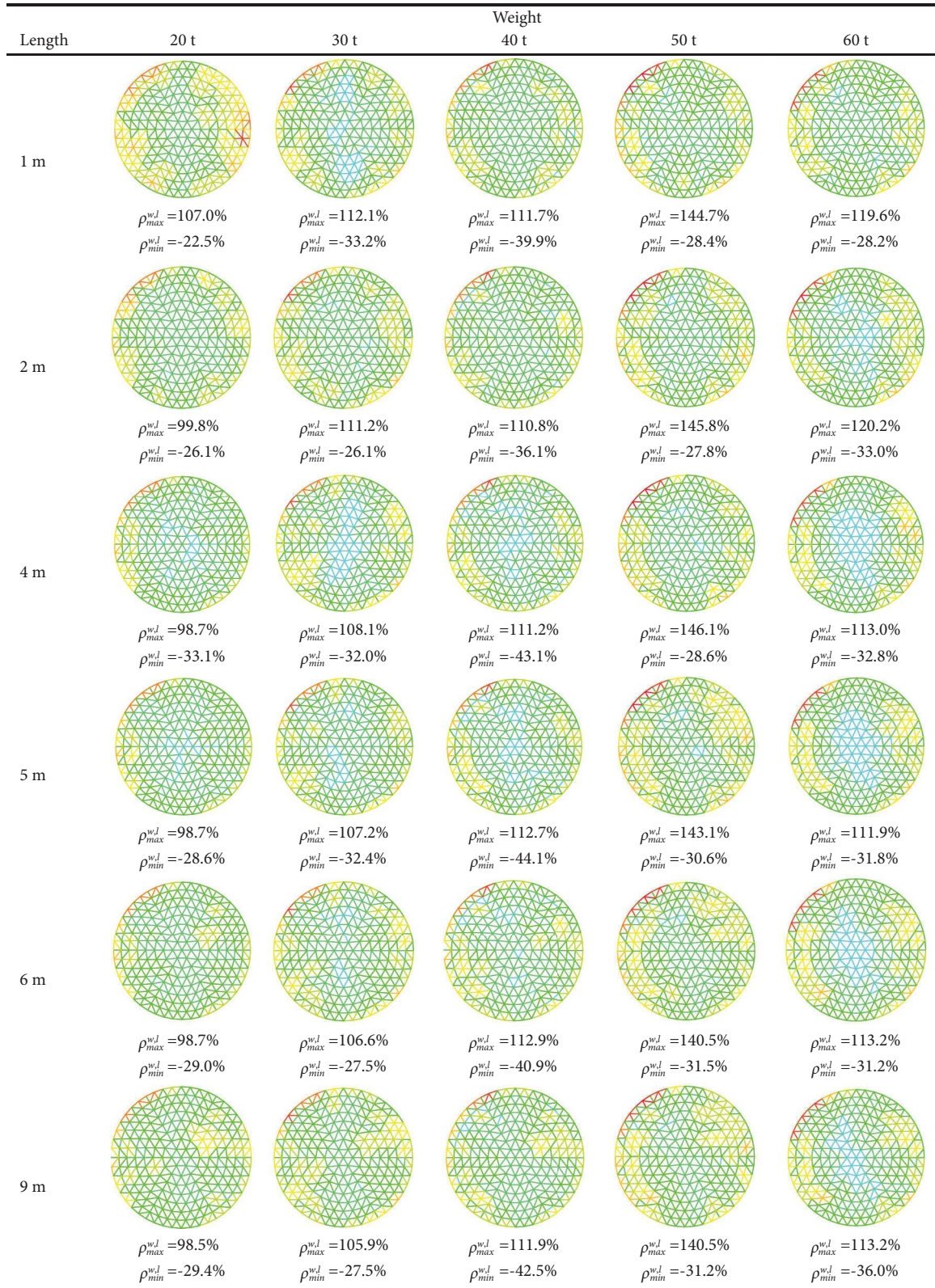


< -80% -60% -40% -20% 0% 20% 40% 60% 80% 100% ; $\geq 20\%$

Note: The legend of the contours is shown as

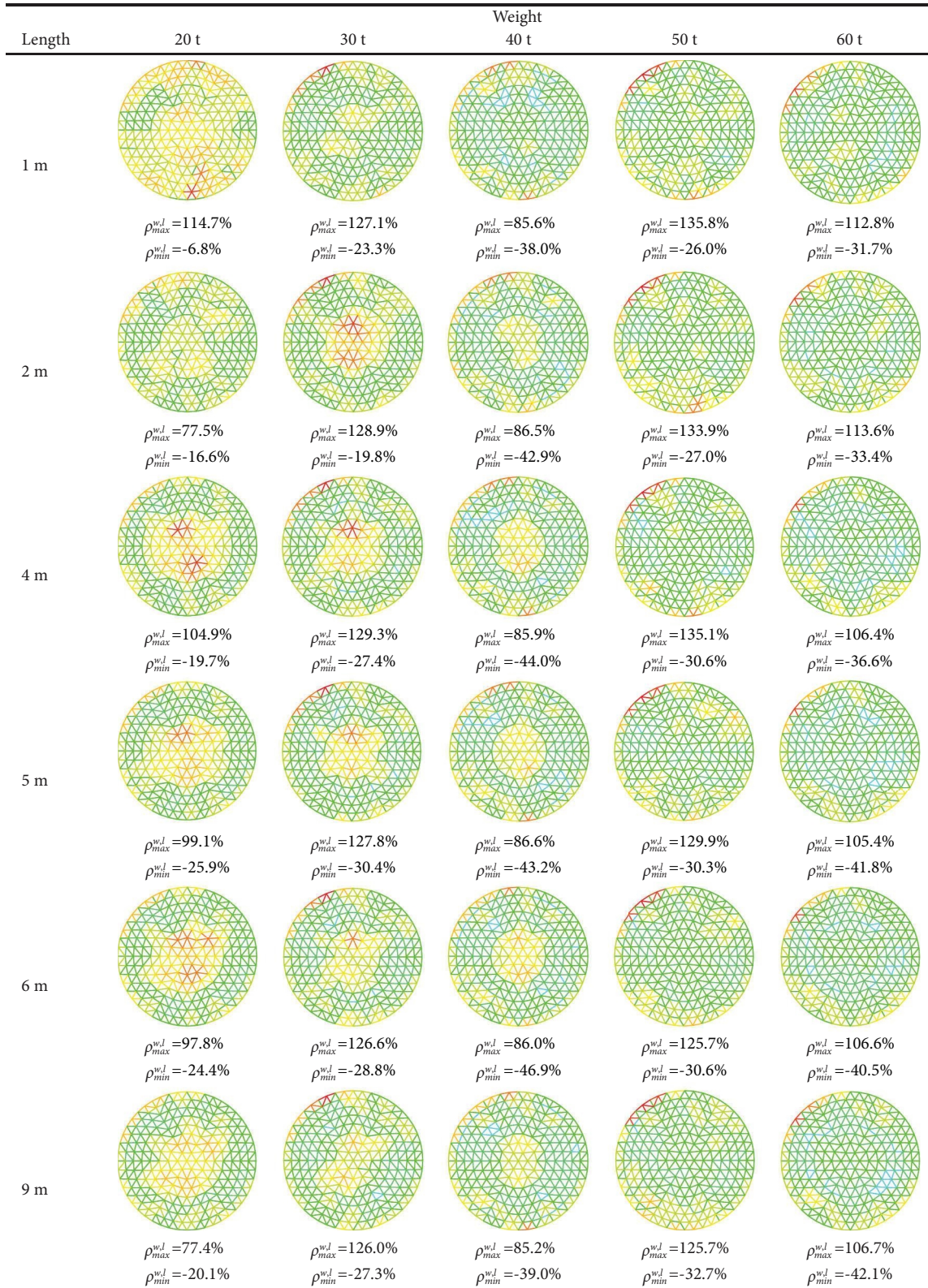


TABLE 3: Contours of the $\rho_{i,\max}^{w,l}$, $\rho_{\max}^{w,l}$, and $\rho_{\min}^{w,l}$ values in the x-direction.



Note: The legend of the contours is shown as

TABLE 4: Contours of the $\rho_{i,\max}^{w,l}$, $\rho_{\max}^{w,l}$, and $\rho_{\min}^{w,l}$ values in the y -direction.

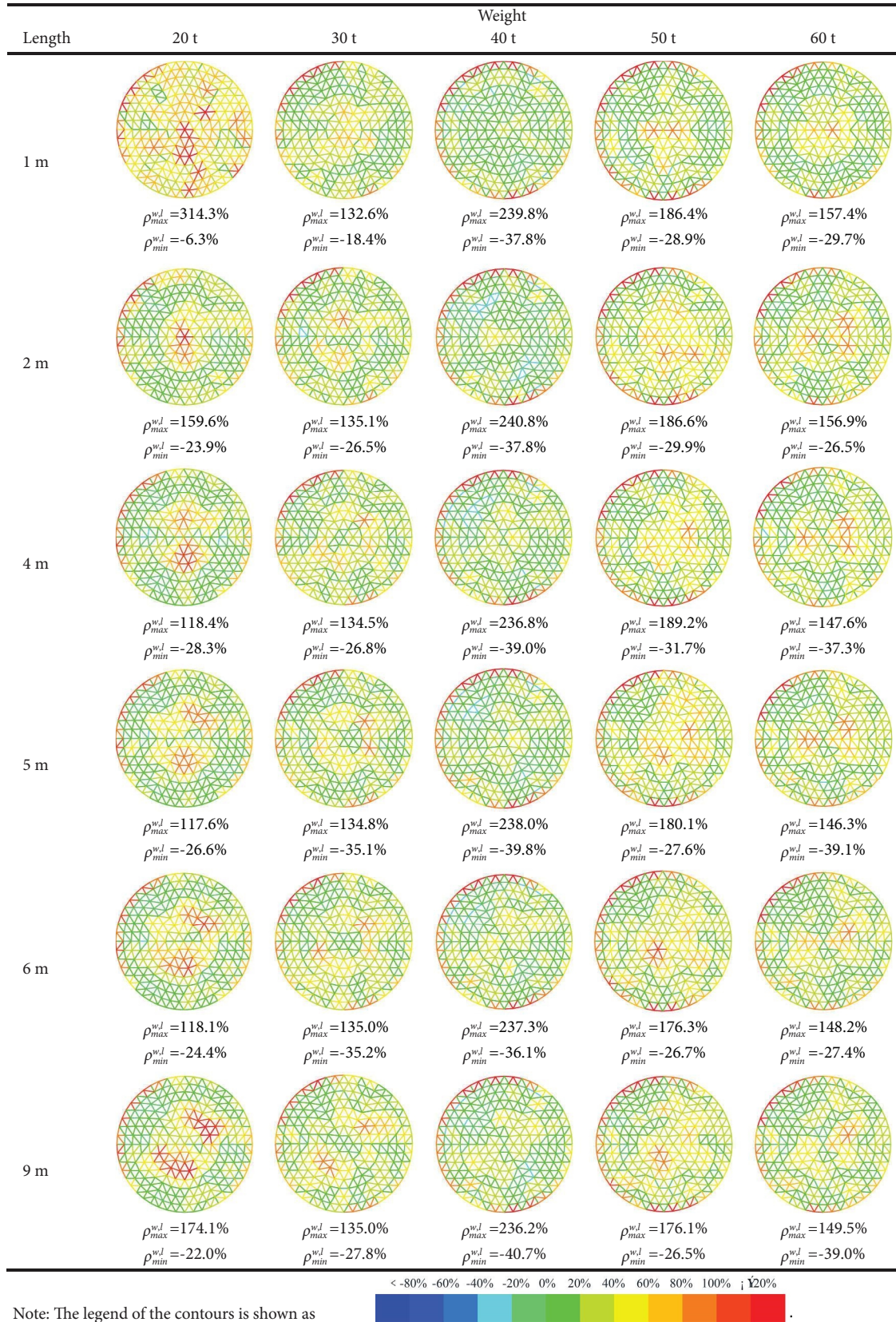


< -80% -60% -40% -20% 0% 20% 40% 60% 80% 100% ; $\geq 20\%$



Note: The legend of the contours is shown as

TABLE 5: Contours of the $\rho_{i,max}^{w,l}$, $\rho_{max}^{w,l}$, and $\rho_{min}^{w,l}$ values in the z-direction.



Note: The legend of the contours is shown as

vertical acceleration is the most affected in the three directions.

Maximum $\rho_{\max}^{w,l}$ in the x -direction appears when w is 50 t and l is 4.0 m. The maximum value of $\rho_{\max}^{w,l}$ in the y -direction appears when the weight is 50 t and the sling length is 1.0 m. Maximum $\rho_{\max}^{w,l}$ in the z -direction appears when the weight is 20 t and the sling length is 1.0 m. Minimum $\rho_{\min}^{w,l}$ appears when the weight is 40 t and the sling length is 5.0 m in the x -direction. Minimum $\rho_{\min}^{w,l}$ appears when w is 40 t and l is 6.0 m in the y -direction. Minimum $\rho_{\min}^{w,l}$ appears when w is 40 t and l is 5.0 m in the z -direction. The influence laws of the CHS weight and the sling length are complicated. This is the same as the influence laws on the axial forces.

It is displayed in Tables 3 and 4 that the region near the boundary is the most affected position in both the x -direction and y -direction. The reason is the horizontal swing effect of the CHS is stimulated under horizontal seismic components. Table 5 shows that the region neighbouring the support platform and the region near the boundary are both greatly affected in the z -direction. It indicates that the vertical impact effect of the CHS affects the acceleration of the reticulated shell the most. This phenomenon shown in Tables 3–5 is consistent with the most affected region for axial forces.

It is suggested that the flexibly suspended model should be used for seismic response analysis. However, if a simplified model is used, the region near the boundary and the region neighbouring the support platform must be concerned and strengthened.

4. Conclusions

The CHS has a significant influence on the seismic response of the single-layer reticulated shell.

In this paper, the seismic performance of the single-layer reticulated shell with a CHS under multiple seismic action is investigated. Flexibly suspended models and simplified models are analysed using the Abaqus software, respectively. The influence of the weight and the sling length of the CHS on the seismic response of the single-layer spherical reticulated shell is also discussed.

Compared with those in the simplified model, the axial forces of some shell members and some nodal acceleration in the flexibly suspended model under multiple seismic excitations would increase by as high as 125% and 315%, respectively. It turns out that seismic responses of the single-layer reticulated shell would be underestimated if a simplified model was used for seismic response analysis.

The parameters including the weight of the CHS and the sling length significantly affect the distribution of the peak axial force change rate of the reticulated shell members and the distribution of the peak acceleration change rate, but the influence laws are complicated. It is hard to find general rules for all single-layer reticulated shells.

The region near the boundary and the region neighbouring the support platform members are the most affected region in the single-layer reticulated shell. The reason why the shell members near the boundary are greatly affected is

the swing effect of the CHS caused by the horizontal component of multiple seismic excitations. The combination of the swing effect caused by the horizontal component and the vertical impact effect caused by the vertical component causes the region neighbouring support platform members to be the most affected part.

It is suggested that the flexibly suspended model should be used for seismic response analysis. The envelope results of flexibly suspended cases taking different CHS weights and sling lengths into account are recommended for structural design. However, if a simplified model is used, the region near the boundary and the region neighbouring the support platform must be concerned and strengthened.

Data Availability

No data were used to support this study.

Conflicts of Interest

The authors declare that there are no conflicts of interest regarding the publication of this paper.

Acknowledgments

This study was funded by the Natural Science Foundation of Shandong (ZR201911030049).

References

- [1] Y. F. Luo, Y. Xiang, and Z. Y. Shen, "Research and application status of seismic analysis techniques for large-span spatial structures," *Chinese Quarterly of Mechanics*, vol. 36, no. 1, pp. 1–10, 2015.
- [2] W. J. Zhang, L. H. Xu, and Y. G. Zhang, "Study on strong earthquake failure mechanism and parameter influence of single-layer spherical reticulated shell," *World Earthquake Engineering*, vol. 35, no. 3, pp. 1–9, 2019.
- [3] J. Zhong, X. D. Zhi, and F. Fan, "Analyses of seismic fragility of single-layer cylindrical reticulated shells under near-fault and far-field ground motions," *China Civil Engineering Journal*, vol. 53, no. S2, pp. 177–182, 2020.
- [4] Y. M. Li, Y. P. Feng, and C. Wang, "Dynamic damage analysis of single-layer reticulated shell structure based on energy principle," *Journal of Building Structure*, vol. 39, no. S2, pp. 366–373, 2018.
- [5] D. W. Kong, L. L. Wang, X. Zhi, and X. D. Zhi, "Seismic performance of column supporting single-layer reticulated domes with friction pendulum bearings," *International Journal of Steel Structures*, vol. 17, no. 2, pp. 471–480, 2017.
- [6] Z. W. Yu, X. D. Zhi, C. Lu, and C. Lu, "Effect of substructures upon failure behavior of steel reticulated domes subjected to the severe earthquake," *Thin-Walled Structures*, vol. 49, no. 9, pp. 1160–1170, 2011.
- [7] K. Zhou, W. X. Ge, X. L. Wang, and N. Nan, "Dynamic stability of K6 single-layer spherical reticulated shell structure under asymmetric load," *Spatial Structure*, vol. 27, no. 3, pp. 17–24+ 31, 2021.
- [8] X. D. Zhi, T. Zhang, W. L. Li, and F. Fan, "Study on the influence of roof system on the stability and seismic response of single-layer spherical reticulated shell," *China Civil Engineering Journal*, vol. 50, no. 2, pp. 19–26, 2017.

- [9] M. Zhang, J. Y. Hou, X. D. Zhi, and W. L. Li, "Effect of initial geometric imperfection modes on seismic performance of single-layer spherical reticulated shell," *Journal of Vibration and Shock*, vol. 40, no. 5, pp. 33–38+74, 2021.
- [10] T. L. Zhang, Y. Ding, and Z. X. Li, "Study on the influence of initial geometric defects on the seismic bearing capacity of single-layer spherical reticulated shell structure," *Spatial Structure*, vol. 24, no. 3, pp. 3–9, 2018.
- [11] X. D. Zhi, Y. N. Zhang, F. Fan, and S. Z. Shen, "Responses of single-layer reticulated domes subject to multiple earthquakes," *Engineering Mechanics*, vol. 35, no. 9, pp. 107–113+125, 2018.
- [12] G. B. Nie, X. D. Zhi, Y. Z. Shang, K. Du, and J. W. Dai, "Seismic performance of single-layer cylindrical latticed shell considering effect of lower supporting structure," *Journal of Building Structures*, vol. 41, no. S1, pp. 10–16, 2020.
- [13] D. B. Yang, C. G. Yun, J. Z. Wu, and Y. G. Zhang, "Study on seismic performance of long-span reticulated shell structure based on separated lower support design," *Journal of Vibration and Shock*, vol. 37, no. 3, pp. 237–242, 2018.
- [14] Z. W. Yu, S. J. Zheng, C. X. Zhen, and H. P. Zhu, "Strong earthquake failure mechanism and seismic vulnerability of single-layer cylindrical aluminum alloy reticulated shell," *Journal of Building Structures*, vol. 41, no. S1, pp. 17–24, 2020.
- [15] Y. Qu, Y. F. Luo, J. J. Cheng, H. Z. Ma, and W. J. Wang, "Two-stage pushover analysis procedure for seismic evaluation of spatial structures under multidimensional earthquake," *Journal of Building Structures*, vol. 43, no. 4, pp. 17–25, 2022.
- [16] X. F. Cai, H. Yu, and C. Nan, "Discussion on design of center-hung scoreboard system for large arena," *Electrical Technology of Intelligent Buildings*, vol. 12, no. 5, pp. 92–98+5, 2018.
- [17] W. Z. Hao, J. Q. Wang, and Q. Li, "Introduction to the center-hung display scheme of a provincial gymnasium," *Video Engineering*, vol. 43, no. 5, pp. 23–25+45, 2019.
- [18] R. J. Liu, C. Wang, and G. Y. Wang, "Analysis of natural vibration characteristics of single layer spherical reticulated shell structure with flexible suspended bucket screen," *Building Structures*, vol. 51, no. s2, pp. 360–365, 2021.
- [19] R. J. Liu, W. Chao, G. Y. Wang, and X. Y. Li, "Influence of center-hung scoreboard on seismic response of single-layer spherical reticulated shell under one-dimensional horizontal earthquake," *Journal of the International Association for Shell and Spatial Structures*, 2022.
- [20] Y. Ding, W. L. Wei, and Z. X. Li, "Multi-dimensional and multi-point non-stationary random seismic response analysis of long-span spatial structures," *Engineering Mechanics*, vol. 24, no. 3, pp. 97–103, 2007.
- [21] C. Wang, *Study on the Influence Law of Gymnasium Hung-Scoreboard on the Seismic Response of Spatial Grid Structure*, Yantai University, Yantai, China, 2022.
- [22] J. Zhang, H. N. Li, and C. Li, "Seismic response of large-span spatial structures under multi-support and multidimensional excitations including rotational components," *Earthquake Engineering and Engineering Vibration*, vol. 20, no. 1, pp. 141–159, 2021.
- [23] J. L. Chen, Z. X. Li, and W. Y. Shu, "Experimental study on mechanical properties of Q345 steel under different strain rates," *Journal of Southeast University (Natural Science Edition)*, vol. 45, no. 6, pp. 1145–1150, 2015.
- [24] *Technical Specification for Space Frame Structures: JGJ 7–2010*, China Architecture & Building Press, Beijing, China, 2010.
- [25] *Code for Seismic Design of Buildings: GB50011–2010*, China Architecture & Building Press, Beijing, China, 2010.
- [26] S. D. Xue, Z. T. Zhao, X. Y. Li et al., "Shaking table test research on the influence of center-hung scoreboard on natural vibration characteristics and seismic response of suspen-dome structures," *Buildings*, vol. 12, no. 8, 2022.
- [27] S. D. Xue, Z. Lu, X. Y. Li et al., "Experimental and numerical investigations on the influence of center-hung scoreboard on dynamic characteristics of suspend-dome structure," *Journal of Building Engineering*, vol. 57, Article ID 104787, 2022.